ADVANCED MATERIALS INTERFACES
www.advmatinterfaces.de

Diffusion of Cation Impurities through Ceria Grain Boundaries

*No Woo Kwak, Dae-Kwang Lim, Seung Jin Jeong, Pilgyu Byeon, Sung-Yoon Chung, and WooChul Jung**

Cerium oxide (ceria) is widely used in relation to solid electrolytes in multiple high-temperature devices, allowing metal components in contact to penetrate into the ceria, especially along the grain boundaries. However, few researchers have concentrated on the migration of metal cations at the operating temperatures (e.g., 600–750 °C) of these devices. Here, the diffusion and solubility of transition metals are investigated through acceptor-doped ceria grain boundaries as a function of the temperature, pO_2, dopant type, and doping concentration. The use of thin-film samples with high grain boundary density levels and time-of-flight secondary ion mass spectrometry with ppb-level chemical resolution enables an accurate analysis of the concentration profiles of metal species present inside the grain boundaries at such low temperatures. Ni, Fe, and Pt migrate unexpectedly rapidly, and the amounts and types of rare-earth dopants have a considerable effect on the diffusion of the transition metal. Furthermore, transition metals (Mn, Fe, Co, Ni, and, Cu) are present at the grain boundaries at substantial solubility levels of $\approx 10^{22}$ cm^{-3}, i.e., 1–2 orders of magnitude greater than in the bulk lattice. The observed dynamic behaviors of transition metals present a new perspective on the performance and durability of ceria-containing applications.

1. Introduction

Rare-earth-doped CeO_2 (ceria) has an excellent oxygen storage/supply capacity and sufficient oxygen ion/proton transport capabilities and is therefore widely used as a catalyst and an electrolyte in applications such as three-way catalysts, hydrocarbon reformers, and solid oxide fuel cells (SOFCs).[1–10] In such devices, ceria is typically in close contact with other metallic components, including transition metals. Thus, metallic cations can penetrate into and/or react with ceria, especially when operating at high temperatures for long periods of time, eventually affecting the performance of the devices. Meanwhile, studies of the diffusion of transition metals into ceria are rare, and the results were only measured at highly elevated temperatures (mostly above 1200 °C).[11–14] This is because the rare-earth-doped ceria is an outstanding oxygen-ion conductor, but cation transport is very sluggish. Moreover, most transition metals have limited solubility in ceria, meaning that they are difficult to detect. Thus far, the migration of these metals has largely been neglected in the temperature range of 600–750 °C, the range at which high-temperature chemical/electrochemical devices typically operate.

It is important to consider that polycrystalline structures with a high grain boundary density are used in most devices. The grain boundary of ceramics can serve as a rapid diffusion pathway for cations. Furthermore, because grain boundaries have more crystallographic defects compared to the bulk lattice, they can accommodate considerably more impurity species.[15–17] For example, Sakai et al.[11] reported that the cation diffusion of Sr in 20%-Gd-doped CeO_2 through the grain boundary is five orders of magnitude faster than that at the bulk interior at 1200 °C. Tuller et al.[18] investigated the grain boundary effect on the diffusion of Ni and Mg using nanocrystalline ceria thin films and found that metal impurities diffuse solely within the grain boundary in the temperature range of 700–800 °C, where bulk diffusion is negligible. Esposito et al.[19–21] reported that the metal solubility and mass diffusion are highly influenced in the doped-ceria system by a chemical reduction from Ce^{4+} to Ce^{3+} at reducing condition, and the aliovalent concentration. We also successfully synthesized various metal nanocatalysts on ceria surfaces via the exceptionally fast grain boundary migration of transition metals.[22] Thus, given that the penetration of transition metal impurities may affect the mechanical, electrical, and electrochemical properties of the host ceria, it is essential to quantify the diffusion kinetics and solubility through the grain boundaries at the target temperature range of 600–750 °C.

In this study, the grain boundary diffusion coefficients and solubility limits of transition metal cations (Mn, Fe, Co, Ni, Cu, and Pt) in rare-earth-doped (Sm, La, Y) ceria are examined. In particular, we want to answer the following three questions, none of which have previously been reported systematically at the temperature range of interest: "how fast do metal cations move along the ceria grain boundary?," "how do rare-earth

Dr. N. W. Kwak,[+] Dr. D.-K. Lim, S. J. Jeong, P. Byeon, Prof. S.-Y. Chung, Prof. W. Jung
Department of Materials Science and Engineering
Korea Advanced Institute of Science and Technology
Daejeon 34141, Republic of Korea
E-mail: wcjung@kaist.ac.kr

The ORCID identification number(s) for the author(s) of this article can be found under https://doi.org/10.1002/admi.202000688.

[+]Present Address: Future Technology Research Center, Corporate R&D, LG Chem Research Park, 188, Moonji-ro, Yuseong-gu, Daejeon, Republic of Korea

DOI: 10.1002/admi.202000688

dopants affect the grain boundary diffusion of metal cations?," and "To what extent can metal cations be contained in the grain boundary compared to the bulk lattice?." One of the difficult aspects of grain boundary diffusion experiments is that the grain boundary thickness can be too narrow to permit the reliable detection of the concentration of transition metals. To solve this problem, we prepared dense polycrystalline thin films with a very high grain boundary density by pulsed laser deposition (PLD) and assessed the amount of diffused metal along the columnar grain boundaries normal to the surface by time-of-flight secondary ion mass spectrometry (ToF-SIMS), a method that offers ppb-level chemical resolutions. It was found that metals diffuse unexpectedly quickly through ceria grain boundaries in the temperature range of 600–750 °C. With 0.5% Sm-doped ceria thin films, Ni cations diffuse to a level exceeding 1 µm within a few days whereas it takes nearly one million years for Ni to diffuse to the same depth in the bulk lattice. Interestingly, the diffusion kinetics of Ni can vary considerably depending on the choice and concentration of the acceptor dopant used as well as the gas atmosphere. Moreover, a considerable amount of transition metal can dissolve in the grain boundaries of ceria, typically at levels one to two orders of magnitude higher compared to the solubility of bulk ceria. The results obtained here are discussed from a scientific and technical point of view.

2. Results and Discussion

2.1. Overview of the Experimental Procedure

The overall experimental procedure performed in this study is as follows. First, we used ceria polycrystalline thin films as a host material and deposited metals on their surfaces by sputtering. We then annealed the sample in air for the metals to diffuse into the host oxide. It is important to determine the annealing temperature so that the metal species only penetrate the grain boundaries of the oxide support; this is often referred to as "heterogeneous doping." According to Harrison's classification, metal ions simultaneously diffuse into the bulk lattice and grain boundary at very high temperatures, but when the homologous temperature is reduced to about a third of the melting point, only grain boundary diffusion occurs.[23] It was found that the targeted temperature range of 600–750 °C is approximately one-third of the homogeneous temperature of ceria, making it possible to effectively observe only cation transport through the grain boundaries while ignoring bulk diffusion.[23,24] Finally, we quantified how much each transition metal entered along the ceria grain boundary by ToF-SIMS. The depth profiles of the transition metals were fitted via 1D diffusion model in a fixed source condition, and the values of the chemical diffusion coefficient were obtained as a function of the temperature, pO_2, the type of dopant, and the doping concentration. Furthermore, the solubility limits of the transition metals at the grain boundaries were determined by analyzing the total concentration when the transition metals were saturated in the ceria grain boundaries. This was done by annealing the samples for a sufficiently long time and at an appropriate temperature.

2.2. Physical and Chemical Characterizations of Ceria Thin Films

In this study, dense and polycrystalline thin films of doped ceria with nanoscale grains were grown on a c-Al_2O_3 (c-plane oriented Al_2O_3) single-crystal substrate via PLD. Three dopants, Sm, La, and Y, were used and their concentrations were measured via inductively coupled plasma mass spectrometry (ICP-MS). The compositions of the dopants in both the targets and the thin films were consistent with nominal values in their concentration range of 0.05% to 20% (Table S1, Supporting Information). The X-ray diffraction pattern of the 0.5% Sm-doped ceria film indicates that the deposited film has a polycrystalline cubic fluorite structure, slightly inclined toward the (111) and (200) orientations (see **Figure 1**a). The intensity ratio between the peaks from the ceria thin film, however, does not differ greatly from that of a powder sample with a random orientation,[25] suggesting that the film is not highly textured. Next, thin diffusion sources (NiO, Fe_3O_4, Co_3O_4, CuO, Mn_3O_4) were deposited onto the ceria films via O_2-reactive sputtering, after which the cations were allowed to diffuse in at temperatures in the range of 600–750 °C. In most cases, metal oxide sources with a thickness of ≈20 nm were used, and only Pt, which does not oxidize readily, was used in the form of metal (see Figure S1, Supporting Information). No change in the XRD peak positions were observed after the high-temperature heat treatment for diffusion (data not shown).

The grain sizes on the surfaces as identified by AFM are 80 ± 15 nm and are relatively monodisperse. The root mean square surface roughness is 1.5 ± 0.6 nm, indicating that the film surface is extremely flat (see Figure 1b). Cross-sectional SEM image obtained from the 0.5% Sm-doped ceria film

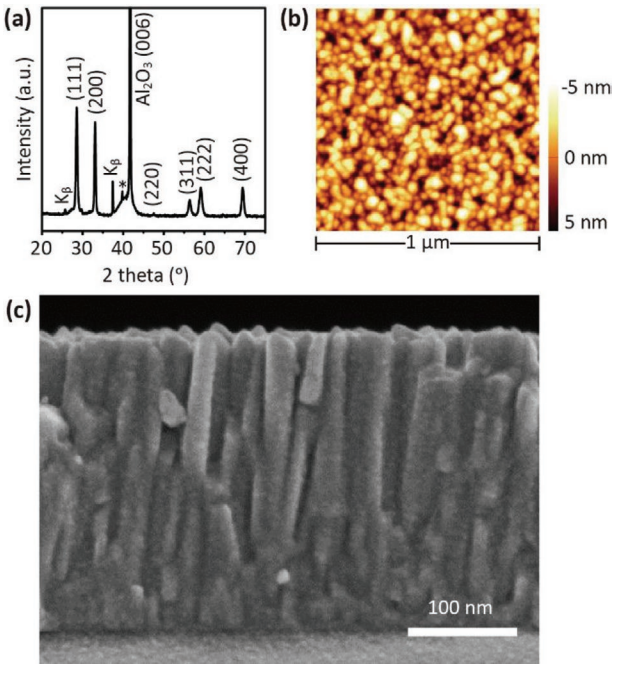

Figure 1. Polycrystalline thin film of Sm 0.5% doped CeO_2 on c-Al_2O_3 (0001) substrate with columnar microstructure: a) X-ray diffraction out-of-plane pattern and * indicates the artefact form aged x-ray tube. b) AFM image of top surface of the ceria film. c) SEM image of cross-section view.

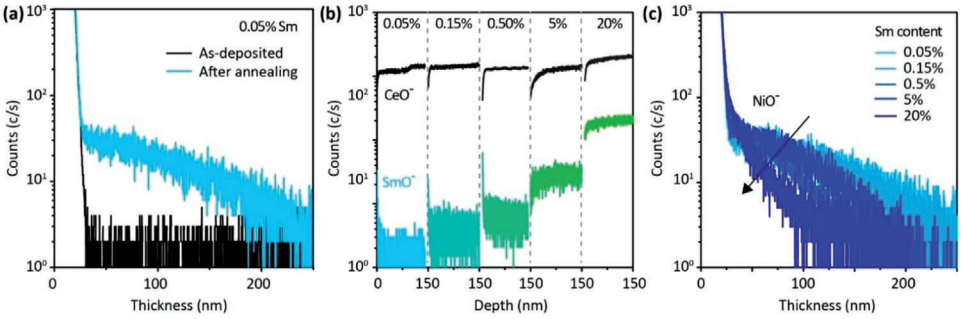

Figure 2. ToF-SIMS spectra of Ni diffusion into the Sm doped ceria film after annealing at 650 °C for 10 h (at high concentration of 0.05%–0.5%) and 20 h (at high concentration of 5%–20%) in oxidizing condition (pO_2 = 0.21 with an Ar balance): depth profile of a) NiO^- SIMS spectrum with as-deposited and annealed, b) CeO^-, SmO^-, and c) NiO^- SIMS spectra depending on Sm content.

shows that the sample has columnar grain boundaries grown in a vertical direction from the substrate to the surface, as intended (see Figure 1c). The use of thin-film samples with a vertically arrayed microstructure and very low surface roughness helps with an accurate analysis of the penetration distance of the metal impurities and in calculations of the volume ratio of the grain boundaries throughout the sample.[26]

2.3. Analysis of Depth Profile by ToF-SIMS

Figure 2a shows the NiO^- SIMS spectra of a NiO|0.05% Sm-doped ceria|Al_2O_3 multilayer sample according to the sample depth. For the as-deposited sample, the intensity of NiO^- falls off sharply at a depth of approximately 20 nm and becomes negligible at deeper levels. In contrast, the heat-treated sample shows similar behavior up to a depth of ≈20 nm, but much clearer NiO^- signals at deeper levels. The initial strong NiO^- spectra come from the NiO diffusion source layer deposited on the surface of the ceria film. In fact, these types of initial spectra were similarly observed in all samples with different diffusion sources or dopant types (see Figure S2, Supporting Information). Based on these observations, it is clear that a considerable amount of impurities from the metal oxide source diffused into the ceria film after the heat treatment for 1.5 to 20 h at 600–750 °C. Here, we use a constant source boundary condition and set the impurity signals in the as-deposited state as a background reference when solving the diffusion equation.

Figure 2b,c shows the SIMS spectra of NiO^-, CeO^-, and SmO^- according to the Sm content. The depth profile of NiO^-, which remains constant with low Sm content (<0.5%), gradually weakens when the Sm concentration exceeds 0.5%. This implies that the Sm added as an acceptor somehow inhibits the diffusion of Ni through the grain boundaries. It is noteworthy that CeO^- and SmO^- maintain a constant intensity level regardless of the depth, unlike NiO^-, and SmO^- gradually increases as the Sm dopant concentration of the thin film increases. These observations are consistent with ICP-MS results (Table S1, Supporting Information) and confirms that a reliable composition profile was being obtained.

2.4. Results of Grain Boundary Diffusion Coefficient

At the relatively low annealing temperatures (600–750 °C) used in this study, the diffusion of transition metal occurs mainly through the grain boundaries of ceria. A high-resolution cross-section analysis of a sample annealed at 700 °C for 5 h under a reducing condition via scanning transmission electron microscopy (STEM) and energy-dispersive X-ray spectroscopy clearly confirms this is the case. The diffused Ni species are selectively concentrated only at the grain boundaries of the host ceria, whereas Ce atoms are spread over the entire area (see the **Figure 3**).[22] Furthermore, the predicted bulk diffusion behavior in this temperature range cannot account for the depth profile of several hundred nanometers, as can be observed in Figure 2. For example, the reported bulk chemical diffusion coefficient of Ni at 700 °C is close to 10^{-29} cm^2 s^{-1} and its effective diffusion length, $2\sqrt{D_{bulk}t}$, is only less than 0.01 Å after 100 h at this temperature.[12,22] Therefore, it is clear that the observed profiles reflect the behavior of the grain boundary chemical diffusion of transition metals, often referred to as "heterogeneous doping."

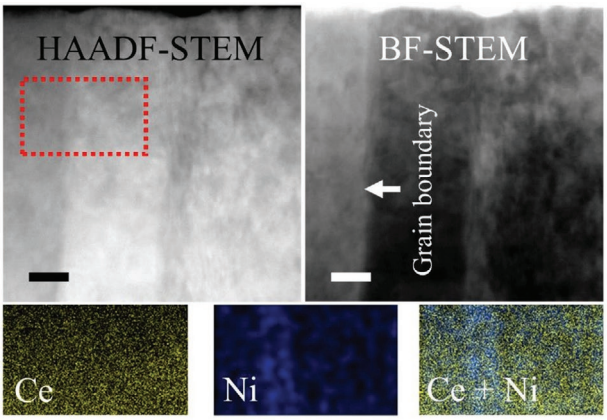

Figure 3. Cross-sectional high-angle annular dark-field (HAADF) and bright-field (BF) scanning transmission electron microscope (STEM) image of samarium doped ceria (SDC) film and energy dispersive X-ray spectroscopy (EDS) mapping results of the highlighted area marked in red (scale bar = 20 nm).

Here, the chemical diffusion coefficient (D^{M}_{GB}) of metal cation impurities along the ceria grain boundaries was obtained by applying a 1D diffusion equation to the impurity depth profile, which is normalized by CeO^{-} as a reference. The specific solution of the diffusion equation for a constant source boundary condition is expressed as Equation S1 (Supporting Information) and has the form of a complementary error function, erfc (x). The fit to the model is in good agreement with the actual SIMS spectrum (see Figure S3, Supporting Information). The absolute values of D^{Ni}_{GB} and the activation enthalpies are shown in **Figure 4**a according to the doping concentration of Sm. It is clear that Ni moves through the grain boundaries very quickly. For example, the D^{Ni}_{GB} value obtained in the 0.05% Sm-doped CeO_2 sample at 700 °C is nearly 10^{13} times higher than the extrapolated value in a bulk single crystal.[19] The diffusion coefficient of Ni remains constant when the concentration of the Sm dopant is lower than 0.5%. However, interestingly, when the Sm concentration is high (>0.5%), the absolute value of D^{Ni}_{GB} decreases and the activation enthalpy increase from 2.2 to 2.9 eV according to the Sm content. This observation indicates that Sm tends to slow the migration of Ni and that Ni is trapped around Sm, especially when the Sm content is high enough. The origin of this phenomenon is difficult to explain because the structure and bonding coordination are unknown at the grain boundaries. Instead, we examined the trapping effect through a classical analytic model reported by Oriani who interpreted this phenomenon in terms of the local equilibrium between mobile and associated diffusing species.[27]

$$D = D_L\left[1+\exp\left(\frac{-\Delta H_{asso}}{kT}\right)\exp\left(\frac{\Delta S_{asso}}{k}\right)\left(\frac{N_x}{N_L}\right)\right]^{-1} \quad (1)$$

where D_L is the diffusion coefficient inside undoped matrix, ΔH_{asso} and ΔS_{asso} are the enthalpy and entropy of association, respectively, k is the Boltzmann constant, and T is the absolute

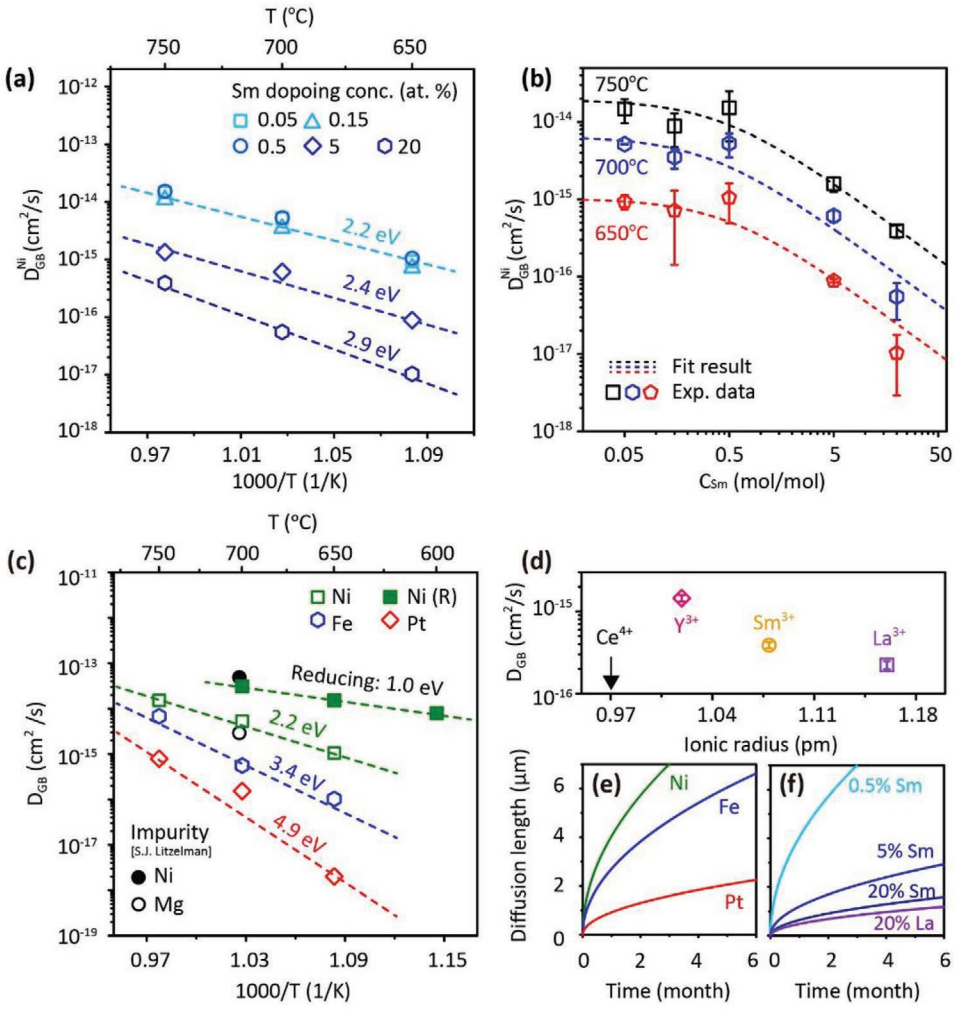

Figure 4. Diffusion coefficients of cation impurities through the ceria grain boundary: Ni diffusivity a) depending on the Sm dopant content and b) as a function of Sm doping concentration, c) diffusivities of Ni, Fe, and Pt as a function of temperature and R indicate reducing condition of $pH_2 = 0.05$ atm with an Ar balance, d) Ni diffusivity at 750 °C for 5 h into Sm, La, and Y 20% doped ceria films as a function of the ionic radius of dopant size, the diffusion length of e) Ni, Fe, and Pt impurities through 0.5% Sm-doped ceria film and of f) Ni impurities diffusion into grain boundaries of 0.5, 5, 20% Sm and 20% La doped ceria as a function of time.

temperature. N_L and N_x represent the number density of normal and trapping (by dopant) sites inside matrix where diffusing species can position, respectively. Assuming that N_x is proportional to Sm doping concentration, the D_{GB}^{Ni} values function of Sm doping concentration at 650–750 °C were best fitted by Equation 1 as shown in Figure 4b. It is noteworthy that the association enthalpy was extracted as 0.5 eV and is consistent with the difference in the activation energy of Ni diffusion between low and high Sm contents, suggesting the existence of some type of defect association. This phenomenon is very similar to those in other diffusion experiments of acceptor-doped CeO_2,[28] $Gd_2Ti_2O_7$,[29] proton diffusion in acceptor-doped $BaZrO_3$,[30] and to hydrogen diffusion in donor- or acceptor-doped Si[31] and these studies carefully concluded that a dopant can associate with diffusing species.

Not only Ni but also other transition metals show very fast diffusion kinetics. Figure 4c shows the diffusivity of Ni, Fe and Pt versus the temperature in 0.5% Sm-doped CeO_2. Ni (0.69 Å), with a relatively small effective ionic size compared to the others listed in figure, diffuses about 10 and 500 times faster than Fe (0.78 Å; high spin) and Pt (0.80 Å) at 650 °C,[32] suggesting that this diffusion kinetics of a transition metal through a ceria grain boundary strongly related to the ionic radius. These results are similar with diffusion in ZrO_2 system, having same fluorite structure identical to that in this study. Kowalski et al.[33] and Kilo et al.[34] reported that the cation migration energy is mainly ruled by both the ionic radius and ionic charge in ZrO_2-based materials according to their corresponding experimental and computer modeling. Indeed, the impurity diffusivity values obtained in this study are in good agreement with those of Ni and Mg reported through ceria grain boundaries under similar conditions within reasonable margins of error.[18] The diffusion rate is in the order of Ni > Fe > Pt, and the activation enthalpy gradually increases from 2.2 eV (Ni) to 3.4 eV (Fe) and to 4.9 eV (Pt). Interestingly, cation diffusion can be controlled by not only the type of metal source used but also by the heat treatment atmosphere. With regard to Ni chemical diffusion, D_{GB}^{Ni} in a reducing atmosphere ($pH_2 = 0.05$ with an Ar balance), a similar condition with a SOFC anode is 16 times higher than the values under an oxidation condition at 650 °C with a decrease in the activation energy from 2.2 to 1.0 eV (Table S2, Supporting Information). Thus, these observations suggest that more attention should be paid to the penetration of transition metals when ceria is used as a SOFC anode or as a hydrocarbon reforming catalyst operating in a reducing atmosphere. The origin of this phenomenon is still an open question, but it seems clear that chemical redox has a significant effect on the diffusion of transition metals. Esposito et al.[35] reported that doped ceria under a reducing condition shows higher grain boundary mobility, suggesting that the chemical composition is strongly influenced by the chemical reduction of Gd-doped ceria. Moreover, the cation mobility can be controlled by a defect formation and diffusion mechanism.[36–38] By the way, it should be noted that in this study, we reduced the samples using a mixture gas with 5% hydrogen balanced in Ar, and did not quantitatively control the pO_2 level. Because the pO_2 level in our reactor increases slightly from 3.7×10^{-31} to 1.1×10^{-28} when the temperature is increased from 600 °C to 700 °C (see Table S3, Supporting Information), the activation enthalpy value reported in a reducing atmosphere may be partially underestimated.

Next, we discussed whether these observations suggest an effect of changes in defect equilibria. To explain our observations in terms of bulk defect chemistry, it must be assumed that transition metal cations move along the space-charge layers adjacent to the ceria grain boundaries in the form of point defects. This is feasible because the structure and/or coordination chemistry of the grain boundary is unknown, and defects cannot be defined in the grain boundary core. Given these basic assumptions, two cases. First, transition metals such as Ni are substituted at the Ce site and diffuse via a vacancy mechanism. Because the grain boundaries of acceptor-doped ceria are generally known to be positively charged,[39–41] fast cation diffusion can arise in this case from the accumulation of cation vacancies, which are effectively negative, in the space-charge layers. For example, De Souza et al.[42] recently reported via numerous analyses that this is possible and that the activation enthalpy of grain boundary diffusion can be close to the value of the bulk diffusion. However, Ni vacancies are effectively negative and therefore cannot have attractive interactions with Sm acceptors. Moreover, according to the equilibrium of the Schottky defect formation reaction, it is expected that the lower the pO_2, the lower the concentration of Ce vacancies and the smaller the D(Ni) value. However, these predictions contradict our observations, and the unusually low activation enthalpy values observed in this study are also not described. Alternatively, one may think that transition metal ions migrate dominantly via an interstitial mechanism. In this case, the association with the Sm acceptor can be understood, and it is also expected that the lower the pO_2, the greater the chemical expansion and, consequently, the lower the migration enthalpy of Ni, in good agreement with our observations. However, if Ni is present as a positive charge at the interstitial site, it must be depleted in a region adjacent to the grain boundaries of ceria, which cannot at all explain the extremely fast grain boundary diffusion we observed. Thus, we think that the grain boundary diffusion phenomena observed in this study cannot be understood solely by bulk defect chemistry, and more information is definitely needed regarding the grain boundaries of ceria. We would like to emphasize that reports on the diffusion of transition metals in ceria are very limited, and it is not yet clear how transition metals migrate even in a ceria bulk lattice.

Next, the different bulk dopant type including La and Y are also investigated using 20% content, emphasizing dopant effect for Ni diffusion, on ceria after heat treatment at 750 °C for 3 h. Figure 4d shows the result of the collected D_{GB}^{Ni} according to the dopant type; the diffusivity of the Y-doped sample is higher (1.45×10^{-15} cm^2 S^{-1}) than Sm (3.90×10^{-16} cm^2 S^{-1}) and La (2.23×10^{-16} cm^2 S^{-1}), indicating that the interaction is minimized when the dopant is similar in size to ceria as a host ion. Thus, Y weakly interferes with grain boundary diffusion of Ni comparing to Sm or La. These observations are corresponding with that the association enthalpy of the dopant-vacancy pairs is minimized when the ionic size of the dopant is coming close to the size of the host cation,[43] whereas trivalent dopant having larger ionic size cause the trapping effect at grain boundary.[13]

We also calculated the diffusion length of the cation impurities through the ceria grain boundaries based on the obtained

results (see Figure 4e,f). Typically, metal cation impurities can quickly diffuse into the grain boundary at approximately a few hundred nanometers within a few days, whereas impurity diffusion into the bulk is less than 0.01 Å for same the period.[12,22] Fast diffusion behavior of metals in particular indicates that the ceria grain boundary in devices already contains impurities such as Ni, Fe, and/or Pt, which are transition metals typically used in high-temperature devices such SOFCs and hydrocarbon reformers. This diffusion kinetics information can be useful for predicting device degradation rate or the formation of secondary phase. For example, Ni, a typical SOFC anode component, can penetrate a 7 µm thick ceria electrolyte and reach the cathode in just three months at 750 °C. Importantly, diffusion behavior can controlled during the material design stage, as the extent to which transition metals spread to ceria depends on the presence of additional dopants, just as the addition of Sm suppresses the diffusion of Ni in this study. Lastly, it is noteworthy that the possibility that surface diffusion influenced the results of this study should not be completely ruled out. SEM, TEM, AFM, SIMS analyses confirmed that the acceptor-doped CeO_2 thin films used in this study are dense without any detectable pore channels, but columnar microstructures often form inter-columnar pore channels that can induce the rapid surface diffusion of transition metals.

2.5. Results of Grain Boundary Solubility Limit

We have studied how rapidly transition metals can move along ceria grain boundaries in previous section. Finally, we look at how much metal can be included in the grain boundaries, known as the grain boundary solubility limit. In this case, five different 3d-transition metals (Mn, Fe, Co, Ni, and Cu) were chosen because these metals are often used in contact with ceria in multiple high-temperature electrochemical/chemical devices. Samples deposited with oxide diffusion source layers by reactive sputtering (metal oxide|0.05% Sm-doped CeO_2) were annealed at 750 °C for 24 h, a sufficient time for the SIMS signals to be constant over the thickness of the ceria films (see Figure S4, Supporting Information). The total amount of the transition metals saturated inside the ceria is shown in **Figure 5**a. The CeO^- SIMS signal intensity remains constant in all samples, but those of the transition metals increase significantly after the heat treatment, indicating that a considerable amount of the transition metal exists at the ceria grain boundaries. In fact, the SIMS intensity is proportional to the concentration, but a quantitative analysis of the absolute value of the doping concentration is difficult. To do this, we created reference thin-film samples that have known transition metal bulk concentrations, in this case 0.1%, in a very precise manner and compared their SIMS intensity levels with those of our target samples. The specific calculations for the quantitative concentration analysis conducted here are given in Equation S2 (Supporting Information). Consequently, we were able to obtain the grain boundary solubility level for the five transition metals (see Figure 5b and **Table 1**). Their grain boundary solubility levels were ≈10^{22} cm^{-3}, which is 10 to 100 times larger than that of the bulk lattice. For example, Ni can be dissolved up to 2.5×10^{20} cm^{-3} and 2.3×10^{22} cm^{-3} at the ceria bulk and at the grain boundaries, respectively. This very considerable difference in the solubility means that the grain boundaries play a very important role in the interaction between the ceria and the transition metals. Evidently, we can confirm that the ceria grain boundary serves as a reservoir for storing a large number of impurities as well as the fast pathway where impurities can diffuse.

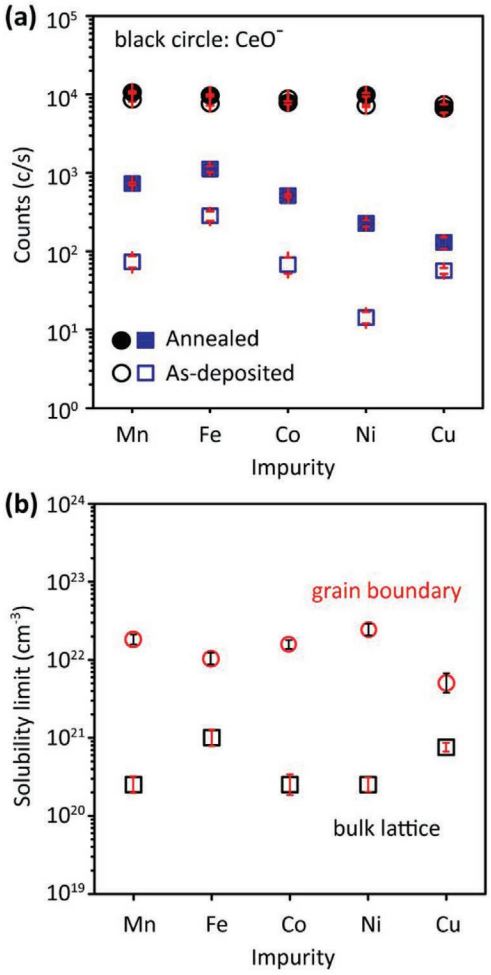

Figure 5. Diffusivity and solubility of impurities inside grain boundary of ceria after annealing at 750 °C in oxidizing condition ($pO_2 = 0.21$ atm with an Ar balance): a) The quantity of ToF-SIMS depth profile of various impurities before/after annealing and b) comparison of the solubility limit of impurities inside ceria bulk lattice and grain boundary after annealing for 24 h.

Table 1. The solubility of impurities inside 0.5% doped CeO_2 grain boundaries after annealing at 750 °C for 24 h.

CeO_2	Mn [cm^{-3}]	Fe [cm^{-3}]	Co [cm^{-3}]	Ni [cm^{-3}]	Cu [cm^{-3}]
Bulk	2.5×10^{20}	1.0×10^{21}	2.5×10^{20}	2.5×10^{20}	7.6×10^{20}
Grain boundary	1.8×10^{22}	1.0×10^{22}	1.5×10^{22}	2.3×10^{22}	5.0×10^{21}

3. Conclusion

In summary, we successfully investigated the diffusion behavior of transition metals into acceptor-doped ceria grain boundaries in the temperature range of 600 to 750 °C. The diffusivities obtained according to the impurity type were in the order of Ni > Fe > Pt, showing fast diffusion along the grain boundary of ceria. The high content of dopant (>0.5% Sm in this study) remarkably inhibited the diffusion of cation impurities through the ceria grain boundaries. The impurity diffusion showed dependence according to the ionic size of the rare-earth dopant used. This effect is confirmed that the impurity diffusion through grain boundary of the ceria doped of Y^{3+} having a similar size to host cation is faster than the case of ceria doped of dopants with larger ion size, such as like Sm^{3+} and La^{3+}. Furthermore, the impurity solubility levels of Mn, Fe, Co, Ni, and Cu at the grain boundary are enormous and are one or two orders higher in magnitude than those in the bulk. These observations reveal the unexpected dynamics of transition metals in high-temperature catalysts/electrolytes containing ceria and provide useful information about the development of high-performance chemical and electrochemical devices.

4. Experimental Section

Target Preparation: $Ce_{1-x}M_xO_{2-\delta}$ (M = Sm, La, and Y with $0.0005 \leq x \leq 0.2$) targets with diameters of 2.5 cm were prepared by a citrate synthesis method using $Ce(NO_3)_3{\cdot}6H_2O$ (JUNSEI, Japan, 99.99%), $Sm(NO_3)_3{\cdot}6H_2O$ (Alfa Aesar, 99.9%), $La(NO_3)_3{\cdot}6H_2O$ (Sigma Aldrich, 99.99%), and $Y(NO_3)_3{\cdot}6H_2O$ (Sigma Aldrich, 99.8%) precursors as starting materials. The precursors were dissolved in deionized water with citric acid (JUNSEI, Japan, 99.7%) at a molar ratio of 1:2.5 (total cations to citric acid). The mixture was forming the gel with persistent stirring at 80 °C and then placed in a heating mantle at 200 °C to dry following to complete burning at 400 °C. The obtained powder was calcined at 900 °C for 10 h in ambient air, milled by a planetary ball-mill in deionized water, and then dried overnight. The powder was uniaxially-pressed to create a pellet and was further cold-pressed at 200 MPa, followed by sintering under air at 1400 °C for 6 h.

Sample Fabrication: The rare-earth-doped CeO_2 thin films were prepared by pulsed laser deposition (PLD) from oxide targets of the respective composition materials and deposited on single crystalline Al_2O_3 substrates (0001) $10 \times 10 \times 6.5$ mm^3 in size (Dasom RNA, Korea). The substrates were initially rinsed with acetone, isopropanol, and deionized water in this sequence. The drying process was carried out using N_2 gas and a hot plate at 100 °C for 3 min. Each cleaned Al_2O_3 substrate was placed in a PLD vacuum chamber with a high vacuum level ($\leq 2 \times 10^{-5}$ Torr). An ablation process was conducted at a substrate temperature of 500 °C using a COMPex 205 KrF excimer laser (LAMBDA PHYSIK, Germany) with emitting at a wavelength of 248 nm, a pulsed laser energy of 250 mJ, and a laser repetition rate of 20 Hz. The procedure of PLD deposition was optimized for CeO_2 thin film and well described in previous research.[26,44] After the deposition step, all of the samples were annealed in air at 700 °C for 10 h using a tube furnace.

Transition metal oxide films and a Pt film as an impurity diffusion source were prepared by DC magnetron sputtering on the top surface of Sm-doped ceria thin film under preciously controlled gas condition (oxide: $pO_2 = 0.5$ atm with an Ar balance, metal: pAr = 1 atm) using 3 in. metal targets (>99.999%, iTASCO, Korea) under DC power of 100 W. The finally created structure is as follows: diffusion source layer|polycrystalline doped ceria film|c-Al_2O_3 substrate. The thicknesses of the impurity layers were held to approximately 20 nm for Mn_3O_4, Fe_3O_4, Co_3O_4, NiO, and CuO and to approximately 210 nm for Pt to ensure good thermal stability.[45] After the impurity deposition process, all samples were annealed in a tube furnace under syngas ($pO_2 = 0.21$ or $pH_2 = 0.05$ atm with an Ar balance) in an intermediate temperature range (600–750 °C) for 1.5–24 h to interdiffuse at the grain boundaries of the rare-earth-doped CeO_2 thin film, which vertically-oriented nanograins.

Characterization Method: X-ray diffraction (XRD) measurements of the films deposited onto the Al_2O_3 (0001) substrates were carried out using a Bragg-Brentano diffractometer (Rigaku Ultima IV, Japan) with Cu-Kα radiation (λ = 1.5406 Å). The microstructure and thickness of the thin films were examined by observing cross-sectional images of the films using a field-emission scanning electron microscope (FE-SEM; SU8230, Hitachi) with an acceleration voltage of 3 kV and an emission current of 2 μA without a surface coating on the samples. The grain size and surface roughness of films were characterized by atomic force microscopy (AFM) using a PSIA (NX-10) device in tapping mode. The chemical composition of the initial powders and the deposited films were measured using an (7700S, Agilent) inductively coupled plasma mass spectrometer (ICP-MS) in the He mode, after dissolution in a (HNO_3:HCL = 7:3) solution at 200 °C for 30 min. Scanning transmission electron microscopy (STEM) was carried out at 200 kV combined with energy dispersive spectrometry (EDS) to identify the chemical composition distribution of the ceria grain boundary. A four windowless silicon drift detectors (SDD) EDS system (Super X) was used as an EDS detector.

Depth Profile Analysis: The impurity diffusion profiles of the poly-crystalline ceria thin film samples were analyzed before/after the annealing process by time-of-flight secondary ion mass spectroscopy (ToF-SIMS; TOF-SIMS5, Germany). Here, 25 keV Bi^+ clusters with a raster of 256×256 measured points scanned over an area of 500×500 μm^2 were used to generate negatively charged secondary ions, and the secondary ion intensity levels of all relevant isotopes and clusters were analyzed simultaneously. For depth-profiling, 1 keV O^{2+} ions (800×800 μm^2) were used in non-interlaced mode (analyze 1 frame, sputter 3 s, pause 4 s) for sequential ablation of the surface between measurements of the mass spectra. A low-energy electron flood gun was employed for charge compensation. After measurements, the crater depths of every sample were determined using a surface profiler (α-Step IQ).

Supporting Information

Supporting Information is available from the Wiley Online Library or from the author.

Acknowledgements

N.W.K. and D.-K.L. contributed equally to this study. This study was supported financially by NanoMaterial Technology Development Program (NRF-2017M3A7B4049547), Basic Science Research Program (NRF-2019R1A2C2006006), Global Frontier R&D Program (2011-0031569), Energy Cloud R&D Program (NRF-2019M3F2A1072236), and Nano-Future Material Original Technology Program (NRF-2020M3H4A1A01086906) through the National Research Foundation of Korea (NRF) funded by the Ministry of Science, ICT and Future Planning.

Conflict of Interest

The authors declare no conflict of interest.

Keywords

cation diffusion, ceria, grain boundary diffusion, thin-films, ToF-SIMS

Received: April 21, 2020
Revised: July 4, 2020
Published online:

[1] W. C. Chueh, C. Falter, M. Abbott, D. Scipio, P. Furler, S. M. Haile, A. Steinfeld, *Science* **2010**, *330*, 1797.
[2] K. Kim, J. D. Yoo, S. Lee, M. Bae, J. Bae, W. Jung, J. W. Han, *ACS Appl. Mater. Interfaces* **2017**, *9*, 15449.
[3] G. L. Lee, J. H. Park, Y. G. Shul, *Nat. Commun.* **2014**, *5*, 4045.
[4] Q. Wang, B. Zhao, G. Li, R. Zhou, *Environ. Sci. Technol.* **2010**, *44*, 3870.
[5] E. P. Murray, T. Tsai, S. A. Barnett, *Nature* **1999**, *400*, 469.
[6] H. G. Seo, Y. Choi, B. Koo, A. Jang, W. Jung, *J. Mater. Chem. A* **2016**, *4*, 9394.
[7] S. Lee, J. Seo, W. Jung, *Nanoscale* **2016**, *8*, 10219.
[8] J. Wang, X. Xiao, Y. Liu, K. Pan, H. Pang, S. Wei, *J. Mater. Chem. A* **2019**, *7*, 17675.
[9] Y. Chen, Y. Zhang, J. Baker, P. Majumdar, Z. Yang, M. Han, F. Chen, *ACS Appl. Mater. Interfaces* **2014**, *6*, 5130.
[10] R. Rao, M. Yang, C. Li, H. Dong, S. Fang, A. Zhang, *J. Mater. Chem. A* **2015**, *3*, 782.
[11] N. Sakai, H. Kishimoto, K. Yamaji, T. Horita, M. E. Brito, H. Yokokawa, *J. Electrochem. Soc.* **2007**, *154*, B1331.
[12] J. D. Sirman, D. Waller, J. A. Kilner, *Solid Oxide Fuel Cells V*, The Electrochemical Society, Pennington, NJ **1997**.
[13] P.-L. Chen, I.-W. Chen, *J. Am. Ceram. Soc.* **1994**, *77*, 2289.
[14] J. C. De Vero, K. Develos-Bagarinao, H. Matsuda, H. Kishimoto, T. Ishiyama, K. Yamaji, T. Horita, H. Yokokawa, *Solid State Ionics* **2018**, *314*, 165.
[15] B. Feng, I. Sugiyama, H. Hojo, H. Ohta, N. Shibata, Y. Ikuhara, *Sci. Rep.* **2016**, *6*, 20288.
[16] C. D. Terwilliger, Y.-M. Chiang, *Acta Metall. Mater.* **1995**, *43*, 319.
[17] W. D. Kingery, *Pure Appl. Chem.* **1984**, *56*, 1703.
[18] S. J. Litzelman, R. A. De Souza, B. Butz, H. L. Tuller, M. Martin, D. Gerthsen, *J. Electroceram.* **2009**, *22*, 405.
[19] D. W. Ni, D. Z. de Florio, D. Marani, A. Kaiser, V. B. Tinti, V. Esposito, *J. Mater. Chem. A* **2015**, *3*, 18835.
[20] V. Esposito, D. W. Ni, S. Sanna, F. Gualandris, N. Pryds, *RSC Adv.* **2017**, *7*, 13784.
[21] V. Esposito, D. W. Ni, D. Marani, F. Teocoli, K. Thydén, D. Z. de Florio, F. C. Fonseca, *J. Mater. Chem. A* **2016**, *4*, 16871.
[22] N. W. Kwak, S. J. Jeong, H. G. Seo, S. Lee, Y. Kim, J. K. Kim, P. Byeon, S.-Y. Chung, W. Jung, *Nat. Commun.* **2018**, *9*, 4829.
[23] L. G. Harrison, *Trans. Faraday Soc.* **1961**, *57*, 1191.
[24] D. Prokoshkina, V. A. Esin, G. Wilde, S. V. Divinski, *Acta Mater.* **2013**, *61*, 5188.
[25] S. Omar, E. D. Wachsman, J. C. Nino, *Solid State Ionics* **2008**, *178*, 1890.
[26] N. W. Kwak, W. Jung, *Acta Mater.* **2016**, *108*, 271.
[27] R. A. Oriani, *Acta Metall.* **1970**, *18*, 147.
[28] J. Faber, C. Geoffroy, A. Roux, A. Sylvestre, P. Abélard, *Appl. Phys. A* **1989**, *49*, 225.
[29] S. A. Kramer, H. L. Tuller, *Solid State Ionics* **1995**, *82*, 15.
[30] Y. Yamazaki, F. Blanc, Y. Okuyama, L. Buannic, J. C. Lucio-Vega, C. P. Grey, S. M. Haile, *Nat. Mater.* **2013**, *12*, 647.
[31] G. G. DeLeo, W. B. Fowler, T. M. Sudol, K. J. O'Brien, *Phys. Rev. B* **1990**, *41*, 7581.
[32] R. D. Shannon, *Acta Crystallogr.* **1976**, *32*, 751.
[33] K. Kowalski, A. Bernasik, A. Sadowski, *J. Eur. Ceram. Soc.* **2000**, *20*, 2095.
[34] M. Kilo, R. A. Jackson, G. Borchardt, *Philos. Mag.* **2003**, *83*, 3309.
[35] V. Esposito, D. W. Ni, Z. He, W. Zhang, A. S. Prasad, J. A. Glasscock, C. Chatzichristodoulou, S. Ramousse, A. Kaiser, *Acta Mater.* **2013**, *61*, 6290.
[36] I.-W. Chen, X.-H. Wang, *Nature* **2000**, *404*, 168.
[37] I.-W. Chen, *Interface Sci.* **2000**, *8*, 147.
[38] K. Une, *J. Nucl. Mater.* **1988**, *158*, 210.
[39] X. Guo, W. Sigle, J. Maier, *J. Am. Ceram. Soc.* **2003**, *86*, 77.
[40] X. Gue, R. Waser, *Prog. Mater. Sci.* **2006**, *51*, 151.
[41] A. Tschope, *J. Electroceram.* **2005**, *14*, 5.
[42] J. P. Parras, R. A. De Souza, *Acta Mater.* **2020**, *195*, 383.
[43] J. A. Kilner, *Solid State Ionics* **2000**, *129*, 13.
[44] T.-S. Oh, Y. S. Tokpanov, Y. Hao, W. Jung, S. M. Haile, *J. Appl. Phys.* **2012**, *112*, 103535.
[45] H. G. Seo, Y. Choi, W. Jung, *Adv. Energy Mater.* **2018**, *8*, 1703647.

